Mon. Not. R. Astron. Soc. **000**, 000–000 (2001) Printed 5 February 2008 (MN LATEX style file v1.3)

The Influence of the Gravitational Acceleration on the Supernova-Driven Parker Instability.

Adriane Steinacker[1,2] and Yuri A. Shchekinov[1,3]
[1] *Astronomisches Institut, Ruhr-Universität Bochum, D-44780 Bochum, Germany*
E–mail: adriane@duras.arc.nasa.gov
[2] *NASA Ames Research Center, Moffet Field, CA 94035, USA*
[3] *Department of Physics, Rostov State University, 344090 Rostov on Don, Russia*
E–mail: yus@rsuss1.rnd.runnet.ru

accepted

ABSTRACT

Within a framework of 2D magnetohydrodynamic (MHD) simulations, we explore the dynamical regimes initiated by a supernova explosion in a magnetized stratified interstellar medium (ISM). We concentrate on the formation of large scale magnetic structures and outflows connected with the Parker instability. For the sake of simplicity we show only models with a fixed explosion energy corresponding to a single SN occuring in host galaxies with different fixed values of the gravitational acceleration g and different ratios of specific heats. We show that in general depending on these two parameters, three different regimes are possible: *a)* a slowly growing Parker instability on time scales much longer than the galactic rotation period for small g, *b)* the Parker instability growing at roughly the rotation period, which for ratios of specific heats larger than 1 is accompanied by an outflow resulting from the explosion for intermediate g, and *c)* a rapidly growing instability and a strong blowout flow for large g. By means of numerical simulations and analytical estimates we show that the explosion energy and gravitational acceleration which separate the three regimes scale as Eg^2 ∼const in the 2D case. We expect that in the 3D case this scaling law is Eg^3 ∼const. Our simulations demonstrate furthermore, that a single SN explosion can lead to the growth of multiple Parker loops in the disc and large scale magnetic field loops in the halo, extending over 2-3 kpc horizontally and up to 3 kpc vertically above the midplane of the disc.

Key words: MHD – instabilities – ISM: bubbles – kinematics and dynamics – magnetic fields – galaxies: halos

1 INTRODUCTION

Recent observations show the presence of dust in extended haloes of spiral galaxies which in some cases reaches out up to distances of around 2 kpc above the galactic plane (Howk & Savage 1997). The dusty gas clouds can account for 10 % of the total gas mass in the disc. This finding rises the central question of how this material is lifted up to the observed heights. There are arguments against the classical scenario of SN explosions as an efficient mechanism for the transport of material above the disc. An essential requirement to these mechanisms is that they must be soft enough in order to allow the dust grains to survive when being spread over such large scales (a more detailed discussion can be found in Howk & Savage 1997). Finally, the structure of the interstellar medium in the regions of interest may play a role in the transport mechanisms. This structure, in turn, is determined by the dynamical processes which are taking place in the galactic plane. On the one hand, the large scale supershells and holes observed in the Milky Way and in nearby face-on galaxies (Heiles, 1984, Brinks & Bajaja 1986, Puche *et al.* 1992, Kim S. *et al.* 1999, Walter & Brinks 1999), the extended H_α and dust haloes observed in nearby edge-on galaxies (Dettmar 1992, Sofue *et al.* 1994, Howk & Savage 1999, Tüllmann & Dettmar 2000), and the large scale gas outflows in dwarf galaxies (Meurer *et al.* 1992, Martin 1996), are commonly thought to be connected with coherent supernova explosions. On the other hand the large-scale magnetic loop structures observed in edge-on galaxies (Dettmar,

private communication), the rising and falling gas motions above spiral arms (Sofue and Tosa 1974), the loops observed in Orion (and towards the galactic centre (Appenzeller 1974, Sofue 1976, Scalo 1985, Sofue and Handa 1984) and the radio lobes observed in NGC 3079 and NGC 4388 (Duric *et al.* 1983, Hummel *et al.* 1983) are thought to be produced by the Parker instability. The Parker instability is also a possible mechanism for transporting material out of the disc since at nonlinear stages it entraines a large amount of gas on kpc-scales.

The stability of a gaseous configuration partly supported by a parallel stratified magnetic field in the presence of a gravitational field perpendicular to the direction of the magnetic field was first studied quantitatively by Newcomb (1961). He derived the stability criteria and the corresponding growth rates and showed that the instability criteria are generalizations of the Schwarzschild criterion. In a series of papers, Parker (1966, 1967, 1979) has discussed the instability in the context of the Galactic disc, based on an equilibrium model with a constant gravitational acceleration, a magnetic field parallel to the galactic plane and stratified in vertical direction, and equipartition between magnetic, thermal and cosmic ray pressures. He found the system to be unstable if the adiabatic index is smaller than a given critical value, which depends on whether the wave vectors of the perturbations are 2- or 3-dimensional and provided the magnetic field is large enough.

Over the past two decades, the details of the Parker instability have been filled in by means of analytical stability analyses and numerical simulations. Additional effects and more physics (such as the inclusion of the rotation state of the galactic disc, the spatial dependence of the gravitational acceleration, and different types of perturbations) have been included in both analytical and numerical investigations. The interested reader is referred to review papers such as those of Mouschovias (1996) and Shibata (1996). Here, we will restrict ourselves to the question of whether, and under which conditions the Parker instability can lead to the formation of the observed looplike structures and gas motions in galaxies, and how it evolves under strongly nonlinear perturbations such as SN explosions. Our studies are restricted to 2-D simulations, and we discuss in section 5 some of the uncertainty in our results arising from this restriction.

A realistic model describing this kind of environment has first been presented by Kamaya *et al.* (1996). They account for both the warm gaseous disc and the hot halo. They used a two-temperature equilibrium model in their 2D numerical simulations of the Parker instability triggered by a supernova explosion taking place in the galactic plane. Under realistic conditions, this kind of perturbation is most likely to be the reason for triggering the instability, rather then the sinusoidal perturbations which are commonly assumed. Based on this model, they studied the effect of two values of the ratio of specific heats and different energy input for the explosion on the instability, but did not discuss the influence of different values of the gravitational acceleration on the growth of the instability (Horiuchi *et al.* 1988, Matsumoto *et al.* 1988, Giz & Shu 1993, Kamaya *et al.* 1997, King, Hong & Ryu 1997). The most recent results on the influence of a spatially dependent gravitational acceleration on the evolution of the Parker instability has been presented by Kim & Hong (1998) and Kim *et al.* (2000). The initial vertical density and gravitational acceleration distributions are chosen such that the system is in equilibrium under the assumption of isothermality. Most importantly, the gravitational acceleration reproduces the profile which can be derived from observations of the spatial density distribution and velocity-distance data (Oort 1960, Bahcall 1984, Kuijken & Gilmore 1989), with $g = 4 \times 10^{-9}$ cm s^{-2} at a height of 500 pc above the disc midplane.

The gravitational acceleration is a parameter that can vary widely from galaxy to galaxy. It is known (van der Kruit & Searl 1981) that all disc galaxies have approximately equal thickness of stellar discs, while the velocity dispersion of stars varies in a wide range (Bottema 1995), and as soon as they are self-gravitating the gravitational acceleration must vary as σ^{-2}. Additional evidences can be found in observations of HI in nearby dwarf galaxies, where the observed HI scale heights differ considerably from galaxy to galaxy: 625 pc for Holmberg II galaxy (Puche *et al.* 1992), 350 pc for IC 2574 (Walter & Brinks 1999), 180 pc for the Large Magellanic Cloud (LMC) (Kim S. *et al.* 1999) – while the velocity dispersion of gas varies in a very narrow range around $\sigma_g \simeq 8$ km s^{-1}. On the other hand, the growth rate of the Parker instability and the critical wavelength for instability are inversely proportional to the gravitational acceleration, the latter being important with regards to the perturbations applied to trigger the instability. Thus, in order to understand the vertical distribution of gas and magnetic fields in the haloes of galaxies, the evolution of large scale MHD perturbations in the ISM must be studied for different values of the gravitational potential.

A SN explosion presents a nonlinear time and space dependent perturbation. Its effect on the growth of the instability can be different from the usual sinusoidal perturbations and depends essentially on the dynamics of the explosion. The energy input from SNe explosions (normally clustered in OB associations) is recognized to play a dominant role in structuring the ISM and its overal dynamics in galaxies on scales up to tens of kpc. The standard scenario for producing large scale motions by SNe involves the formation of a superbubble blown out into the gaseous halo or widely expanding within the disc (Tomisaka & Ikeuchi 1986, Tenorio-Tagle *et al.* 1987, Mac Low *et al.* 1989, Palouš *et al.* 1990, Mac Low & Ferrara 1999). When a superbubble expands into a non-magnetized ISM, the condition for a blow-out to occur requires the expansion to remain supersonic until it reaches a vertical distance of about two to three scale heights of the gas distribution (Kovalenko & Shchekinov 1985, Mac Low & McCray 1988). However, in the presence of a magnetic field the situation changes crucially. Bernstein & Kulsrud (1965) and Kulsrud *et al.* (1965) first addressed the question of how a spatially uniform magnetic field can affect the dynamics of a SN explosion. Subsequent studies by Giuliani (1982) and Ferriére *et al.* (1991) have contributed to the understanding of different aspects of the dynamics of a SN remnant in a uniform magnetic field. The main conclusion

that can be drawn from these studies is that the magnetic pressure supresses the expansion of a remnant perpendicular to the field lines, and thus one can expect that in the presence of magnetic field the energy released by SN explosions is confined in the galactic disc. Tomisaka (1990) concluded from his numerical study that a magnetic field with a standard strength $B_0 = 5$ μG provides confinement of the bubbles with typical mechanical luminosity of $L \sim 3 \times 10^{37}$ erg s^{-1}. Quite recently, Tomisaka (1998) has described numerically the dynamics of a superbubble in a vertically stratified magnetic field, specifically addressing the question of whether a superbubble is blown out or remains confined in the disc. He concludes that despite the strong influence of the magnetic tension perpendicular to the field lines, the expansion of superbubbles in vertical direction is supressed much less than previously assumed and is kinematically similar to the hydrodynamical case.

One of the most important feature in the dynamics of superbubbles in a magnetized ISM is that as a result of the magnetic field compression by the shock front, magnetosonic waves are driven ahead of the front (Mineshige et al. 1993). The separation between the magnetosonic wave and the shock front depends on the ratio of the Alfvén velocity to the shock velocity, and increases when the shock is slowing down. Thus, at late stages in the expansion of a superbubble the magnetosonic front can disturb the magnetic field and gas on large scales, much larger than the radius of a bubble, which in turn can initiate the Parker instability when the characteristic radius of the magnetosonic front is comparable to the critical wavelength. Once this condition is fulfilled, the flow associated with the Parker instability drags out the material driven by the superbubble thus favouring its vertical expansion.

In this paper we will concentrate on the role of the gravitational acceleration and the ratio of specific heats on the Parker instability triggered by a point explosion with emphasis on the possible interconnection between the supernova explosion and the Parker instability by using *a)* an isothermal model and *b)* a two-temperature model accounting for both the galactic disc and the halo. In the framework of 2D MHD, we will show that in general there are three different regimes depending on the gravitational acceleration in the disc and on the ratio of specific heats: 1) When the gravitational acceleration is below a certain value, a SN explosion initiates a slowly growing Parker instability on time scales much larger than the galactic rotation period; 2) For large values of the gravitational acceleration the explosion drives a shock wave which initiates a rapidly growing Parker instability with growth rates comparable to typical values of the galactic free-fall time; 3) For $g \geq 4.5 \times 10^{-9}$ cm s^{-2}, and provided the ratio of specific heats is larger than the isothermal value, the Parker instability can amplify the blowout flow – the resulting magnetic structures and gas dynamics are a product of the dynamical interaction of these two processes. In all cases we start with the most favourable adiabatic index for the evolution of both processes (close to isothermal).

The paper is organized as follows: in Section 2 we describe our initial model and numerical method, in Section 3 we qualitatively analyse the possible regimes of the Parker instability by means of energy estimates, in Section 4 we present our results and we close in Section 5 with the discussion of the results and their possible astrophysical implications. A summary of the results is presented in Section 6.

2 INITIAL MODEL AND NUMERICAL METHOD

The dynamics of the investigated system is described whithin the framework of ideal MHD simulations, by assuming the gravitational acceleration to be constant. This is a simplifying assumption, which we only use in order to keep track of the behaviour of the system, and in favour of other important assumptions (*e.g.*to account for the interaction between disc and halo), work with a spatially dependent gravitational acceleration being already underway. We also assume that the thermal and the magnetic pressure are initially equal, *i.e.* the plasma beta $\beta = P_{th}/P_{mag}$ is 1, where P_{th} is the thermal gas pressure and $P_{mag} = B^2/(8\pi)$ is the magnetic pressure, and neglect the effect of the cosmic rays. The simulations have been performed using the Nirvana finite difference code (Ziegler 1995, Ziegler et al. 1996), which is based on the same numerical techniques as ZEUS (Stone and Norman 1992). With the above assumptions, the governing equations are:

$$\frac{D\rho}{Dt} + \rho\nabla \cdot \mathbf{v} = 0, \tag{1}$$

$$\rho\frac{D\mathbf{v}}{Dt} = -\nabla p - \rho\mathbf{g} + \frac{1}{4\pi}(\nabla \times \mathbf{B}) \times \mathbf{B}, \tag{2}$$

$$\rho\frac{D}{Dt}\left(\frac{e}{\rho}\right) = -p\nabla\mathbf{v}, \tag{3}$$

here $D/Dt \equiv \partial/\partial t + \mathbf{v} \cdot \nabla$ denotes the comoving derivative.

$$\frac{\partial\mathbf{B}}{\partial t} = \nabla \times (\mathbf{v} \times \mathbf{B}). \tag{4}$$

The system is closed by a polytropic equation of state

$$p = \kappa\rho^{\gamma}, \tag{5}$$

Table 1. Characteristics of the one-temperature models

run	g (cm/s^2)	γ	H (pc)	λ_c (pc)	λ_m (pc)
1Tg3	$3{\cdot}10^{-9}$	1.05	180	1307	2353
1Tg4.5a	$4.5{\cdot}10^{-9}$	1.05	126	871	1568
1Tg4.5b	$4.5{\cdot}10^{-9}$	1.4	126	1867	3361
1Tg6	$6{\cdot}10^{-9}$	1.05	94.5	653	1175

where all the quantities have their usual meanings. The equations are computed in two dimensions in cartesian coordinates, with x being the longitudinal direction parallel to magnetic field lines. In this paper we restrict ourselves to a constant gravitational acceleration g. Since the perturbation is already nonlinear, space- and time-dependent, and is therefore more complicated than the usually assumed non-localized linear perturbation, we can obtain a better understanding of the qualitative dynamics of the system with regards to basic assumptions, without contaminating effects from spatially varying g. Moreover, it is worth stressing that the gravitational acceleration varies on a scale-height much smaller than the critical wavelength for the Parker instability – for example, in the Milky Way galaxy, g increases from $g = 0$ to $g = 3 \times 10^{-9}$ cm s^{-2} when z varies from $z = 0$ to $z \simeq 200$ pc, and at $z \simeq 600$ pc it reaches $g = 6 \times 10^{-9}$ cm s^{-2} (Kuijken & Gilmore 1989). Therefore, the perturbations of relevant wavelengths, should be largely unaffected by this variation.

Our simulations are starting from either one of the following models, which are based on the assumption for vertical hydrostatic equilibrium:
i) An isothermal model which accounts for the disc only. In this case, the density distribution is an exponentially decreasing function of z:

$$\rho(z) = \rho_0 \exp(-z/H), \tag{6}$$

with the scale height $H = (1+\beta^{-1})c_s^2/g$, where c_s is the isothermal sound speed. For all the runs we have assumed a temperature $T_d = 10^4 K$ and a midplane density of the disc of $n_0 = 1$ cm^{-3}. Three different values for the gravitational acceleration, $g = 3, 4.5$ and 6×10^{-9} cm s^{-2} have been chosen. The parameters for the different runs are summarised in table 1, which also contains the corresponding values for the scale-height and the critical wavelength $\lambda_c = 4\pi H \left[\beta\gamma/(2(1+\beta-\beta\gamma)(1+\beta)-\beta\gamma)\right]^{1/2}$ (Mouschovias 1996). The wavelength of maximum growth for $\beta \sim \gamma \sim 1$ is $\lambda_m = 1.8\lambda_c$ for the instability.
The computational domain ranges from $z_{\min} = 0$ to $z_{\max} = 2100$ pc and $x_{\min} = 0$ to $x_{\max} = 3600$ pc. The total number of grid-zones is $N_x \times N_z = 242 \times 142$, with a grid spacing of $\Delta z = 15$ pc.
ii) A two-temperature model, accounting for both, the disc and its halo. The underlying model corresponds to the one proposed by Kamaya *et al.* (1996). The density-distribution is calculated from a prescribed temperature profile:

$$T(z) = T_d + \frac{(T_c - T_d)}{2}\left[\tanh\left(\frac{\mid z \mid - z_c}{w_{tr}}\right) + 1\right], \tag{7}$$

where w_{tr} is the thickness of a transition layer between disc and corona, T_c is the coronal temperature, and for $z_c \gg w_{tr}$ (in our case $z_c = 1$ kpc and $w_{tr} = 4\Delta z$) T_d can be identified with the midplane temperature of the disc. The above profile leads to the following density distribution:

$$\rho(z) = \rho_0 \frac{T_d}{T(z)} \exp\left[-\frac{\mu I(z)}{2\Re g}\right], \tag{8}$$

where $\mu = 1$ is the molecular mass of the gas in the disc, $\Re$ is the gas constant, and $I(z)$ is a function of T_c, T_d, w_{tr} and the height of the disc z_c which results from the integration. The coronal temperature is $T_c = 2.5 \times 10^5$K, and the temperature in the disc is $T_d = 10^4$K. The rather low value of the temperature in the halo is chosen in order to avoid strong density and temperature jumps, which lead to numerical errors on the interface between disc and halo due to averaging of the physical quantities. However, this is a standard assumption in simulations of the Parker instability in two temperature models (Shibata *et al.* 1989, Matsumoto *et al.* 1993, Kamaya *et al.* 1996). In the real ISM, where radiative cooling can be important on relevant time scales, this temperature corresponds to the peak of the cooling function, and therefore a larger temperature has to be chosen in order to weaken the effects of radiative losses. Shibata *et al.* (1989) have shown that the nonlinear dynamics of the instability initiated by a non-localized sinusoidal perturbation depend only weakly on the ratio T_c/T_d. One can thus expect that for the SN driven Parker instability, the results obtained for $T_c = 2.5 \times 10^5$K provide us with a qualitatively correct understanding for even larger coronal temperatures. The runs performed with this model are summarized in Table 2. We used three different values for the gravitational acceleration, and four values for the ratio of specific heats γ.
The computational domain ranges from $z_{\min} = 0$ to $z_{\max} = 5400$ pc and from $x_{\min} = 0$ to $x_{\max} = 3600$ pc. The total number of grid-zones is $N_x \times N_z = 242 \times 362$, which results in a grid spacing of $\Delta x = \Delta z = 15$ pc. The point explosion is

Table 2. Characteristics of the two-temperature models

run	g (cm/s^2)	γ	H (pc)	λ_c (pc)	λ_m (pc)
2Tg3k1.05	$3{\cdot}10^{-9}$	1.05	180	1307	2353
2Tg3k1.4		1.4		2675	4815
2Tg3k1.75		1.75		—	—
2Tg4.5k1.05	$4.5{\cdot}10^{-9}$	1.05	126	871	1568
2Tg4.5k1.4		1.4		1867	3361
2Tg4.5k1.6		1.6		—	—
2Tg4.5k1.75		1.75		—	—
2Tg6k1.05	$6{\cdot}10^{-9}$	1.05	94.5	653	1175
2Tg6k1.4		1.4		1404	2528
2Tg6k1.6		1.6		—	—

initialized in the origin such that a quantity of thermal energy $E = 10^{51}$erg and a mass of $M_{\rm expl} = 10M_{\odot}$ is concentrated in a cylindrical volume with $r_{\rm cyl} = 43$ pc and height $Y = 1$ kpc. In our simulations the explosion is initialized by an instanteneous energy release – we did not perform computations with a continuous energy input with constant energy ejection rate. Such an approach is justified by the fact that the Parker instability normally develops on time scales longer than the typical time for vigorous evolutionary stages of OB associations.

3 ENERGY REQUIREMENT

In order to understand the dynamics of the Parker instability driven by a SN explosion, we present qualitative estimates for flows produced in a stratified ISM by point explosions. For a point explosion in an exponential non-magnetized atmosphere, the energy required to produce a blow-out can be estimated from the condition that the hot bubble expands supersonically when its radius R_s reaches $\sim 3H$, H being the scale height of the gas distribution (Kovalenko & Shchekinov, 1985, Mac Low & McCray, 1988). This can be understood from a simple estimate of the shock velocity at the upper point of the bubble z, which in an atmosphere with an exponential density distribution $\rho(z) = \rho_0 \exp(-z/H)$ and in 3D is:

$$v(z) \sim \left[\frac{E}{\rho_0}\right]^{1/2} e^{z/2H} z^{-3/2}. \tag{9}$$

This function has a minimum at $z = 3H$ (see Ferrara & Tolstoy 2000). Additionally assuming the bubble to be spherical when $R_s = 3H$ and requiring its expansion velocity at this stage be sonic $v_s = \sqrt{\gamma} c_s$ we obtain

$$E^B_{\rm min} = \left(\frac{5}{2}\right)^2 27 e^{-3} \gamma \rho_0 c_s^2 H^3. \tag{10}$$

The minimum energy for a blow out to occur in a magnetized atmosphere can be estimated by requiring the velocity at $R_s = 3H$ to roughly equal the velocity of the fast magnetosonic wave $v_s \sim \sqrt{v_A^2 + \gamma c_s^2}$, where v_A is the Alfvén velocity. This leads to

$$\begin{aligned} E^B_{\rm min} &= \left(\frac{5}{2}\right)^2 54 e^{-3} (2\beta^{-1} + \gamma) \rho_0 c_s^2 H^3 \\ &\sim \frac{25}{2} (2\beta^{-1} + \gamma) \rho_0 c_s^2 H^3. \end{aligned} \tag{11}$$

Since H is proportional to c_s^2 and to g^{-1}, eq. (11) shows that $E^B_{\rm min}$ strongly depends on the sound speed in the ISM ($\propto c_s^8$), and on the gravitational acceleration in a host galaxy ($\propto g^{-3}$). For $\rho_0 = 1.67 \cdot 10^{-24}$ g cm^{-3}, $T = 10^4$ K, $\gamma = 1.05$ and $g = 3 \times 10^{-9}$ cm s^{-2}, the resulting minimum energy is $E^B_{\rm min} = 4 \times 10^{51}$ erg. Note, that the value of $E^B_{\rm min}$ required to produce a blow-out in the hot halo scales as $E^B_{\rm min} \propto \rho_{\rm h} T_{\rm h}^4$, where $\rho_{\rm h}$ and T_h are the density and temperature of the halo at the disk midplane. At a density corresponding to $n_{\rm h} \sim 0.01$ cm^{-3} and $T_{\rm h} = 25 \times 10^4$ K the minimum energy is $E_B = 3 \times 10^{54}$ erg. This estimate was obtained by neglecting radiative losses, *i.e.* assuming adiabatic expansion, and can thus be considered as a lower limit. This assumption is reasonable. As shock waves expand into a magnetized medium, radiative losses are not particularly severe because the post-shock compression is always weaker in the presence of a magnetic field.

In general, the presence of a magnetic field provides counter-pressure which tends to weaken the propogation of a shock. Within a uniform magnetic field a hot bubble elongates along the field lines, and for a standard energy input or mechanical

luminosity, remains confined in the galactic disc (Tomisaka 1990). In a stratified magnetic field with $\beta = 1$, the situation changes as compared to the non-magnetized case. The most interesting new dynamical feature here is connected with the acceleration of the shock front in the vertical direction and deceleration of the contact discontinuity between the hot bubble and the shocked ISM gas, so that the vertical size of the hot bubble itself is smaller than in the non-magnetized medium, while the thickness of the layer of shocked gas and the vertical size of the disturbed zone is larger (Mineshige, Shibata & Shapiro 1993, Tomisaka 1998). In these calculations the time and spatial scales were restricted to $t \sim 10 - 40$ Myr and $R \sim 0.6 - 1$ kpc, respectively, and the main conclusion of whether a SN produced bubble is confined to the disc or blown out is drawn from the violent early evolutionary stages of the bubble and its associated shock wave. However, at later stages, even a weak shock (or acoustic) wave can stimulate the growth of the Parker instability.

The minimal SN energy required to produce the Parker flow can be derived from the following requirement. The size of the region occupied by the magnetosonic (or Alfvén) wave R_B must grow larger than the critical wavelength of the instability λ_c, and the amplitude of the wave must be large enough to allow the instability to grow on time scales less than the rotation period t_R of the galaxy. In the linear regime, the velocity amplitude grows as $v \sim v_0 \exp(t/t_P)$, where v_0 is the initial amplitude, and $t_P \sim H/c_s$ is the Parker growth time. If the velocity amplitude is to grow to the fast-mode speed by the time t_i, then $v_0 \sim \sqrt{v_A^2 + \gamma c_s^2} \exp(-t_i/t_P)$. Typically, a remnant will expand for about 50 Myr, the value that we will for t_i, and $t_P \sim 10$ Myr. Hence, we require $v_0 \sim 10^{-2}\sqrt{v_A^2 + \gamma c_s^2}$.

In order to estimate the offset time for the Parker instability, we assume that the shock front moves vertically relative to the contact discontinuity with constant velocity equal to the magnetosonic speed v_m and the discontinuity itself propagates with a velocity that coincides by the order of magnitude with the shock velocity of a spherical SN remnant of radius R_s in the Sedov-Taylor phase $v_d \sim v_s = 2R_s/5t$. Thus, vertically, the magnetosonic front reaches the distance:

$$R_z \simeq R_s + v_m t = R_s \left[1 + \frac{2}{5}\frac{(v_A^2 + \gamma c_s^2)^{1/2}}{v_s}\right], \tag{12}$$

where R_s is the radius of the bubble (assumed spherical), and v_s is the shock velocity. Here the expansion time, $t = 2R_s/5v_s$, for an adiabatic bubble has been substituted. Horizontally, the shock front propagates with the Alfvén velocity and reaches the distance:

$$R_x \simeq R_s + v_A t \simeq R_s \left[1 + \frac{2}{5}\frac{v_A}{v_s}\right]. \tag{13}$$

We assume that when $2R_B = 2\sqrt{R_z^2 + R_x^2} = \lambda_c$, the Parker instability begins to grow. The minimum energy can then be obtained by assuming the shock wave is weak at this stage, *i.e.* $v_s \sim \sqrt{v_A^2 + \gamma c_s^2}$. For $\beta = 1$, this leads to $R_B \simeq 2R_s$, and thus the condition for the Parker instability to grow is $R_s \simeq \lambda_c/4$, or $R_s \simeq 1.8H$. Substituting this value into Eq. (9) for $v(z = 1.8H) \sim \sqrt{v_A^2 + \gamma c_s^2} \exp(-t_R/t_P)$, we obtain

$$E_{\rm min}^P \sim \left(\frac{5}{2}\right)^2 (2\beta^{-1} + \gamma) \exp(-2t_R/t_P)\rho_0 c_s^2 H^3. \tag{14}$$

By comparing (11) and (14) we see that in the presence of a stratified magnetic field with $\beta \sim 1$, the explosion energy required to initiate the Parker instability is much less than the explosion energy required to produce a blow out. For $t_R \sim 50$ Myr and $t_P \sim 10$ Myr, $E_{\rm min}^P$ can be only $\sim 10^{-4}$ $E_{\rm min}^B$ in the one-temperature model, and $\sim 0.1 E_{\rm min}^B$ in a two-temperature model with $t_P \sim 50$ Myr in the halo. This energy can be considered as an upper limit if we realize that even subsonic (slow magnetosonic) waves can be amplified in an atmosphere with a decreasing density profile. In an exponential atmosphere the velocity amplitude of acoustic waves increases as (see Lamb 1932),

$$v \propto e^{z/2H}. \tag{15}$$

When the Parker instability initiated by magnetosonic perturbations starts to grow, the amplification can be stronger due to the fact that the flow associated with the instability removes gas from the upper parts of the forming loop and the perturbation propagates in a medium with a temporally decreasing density. If we assume a density decrease described by $\rho \propto \exp(-t/t_P)$, then the velocity amplitude of the magnetosonic wave can grow as

$$v \propto \exp \frac{z}{2H} + \frac{t}{2t_P}. \tag{16}$$

As a result, a secondary shock wave can build up in response to the subsequent steepening of the front of the magnetosonic wave. Such secondary shocks appear in the numerical simulations shown in Section 5.

In the 2D case, the expansion law for a shell produced by a point explosion is given by

$$v(z) \simeq \frac{1}{2}\left[\frac{E}{\rho_0}\right]^{1/2} e^{z/2H} z^{-1}, \tag{17}$$

which leads to the estimate for the minimal blow out energy (equivalent to Eq. 9) in the 3D case of:

$$\varepsilon^B = \frac{E^B}{Y} \sim 2(2\beta^{-1} + \gamma)\rho_0 c_s^2 H^2, \tag{18}$$

and to the minimal energy for the Parker instability (equivalent to Eq. 14 of

$$\varepsilon^P = \frac{E^P}{Y} \sim 2(2\beta^{-1} + \gamma)\exp(-t_R/t_P)\rho_0 c_s^2 H^2, \tag{19}$$

where ε is the explosion energy per unit length and Y is the size of the computational domain in y.

4 RESULTS

4.1 One temperature model

In order to describe the actual situation in a galactic environment in a realistic way, one needs to account for the observed difference in temperature between the disc and the halo. Nevertheless, in order to help fix ideas, we have performed several runs within the framework of an isothermal distribution. We were motivated by the fact that most of the previous numerical studies of the Parker instability initiated by non-localized (smoothly distributed) large scale perturbations have been conducted within the confines of an isothermal ISM (Basu, Mouschovias & Paleologou 1997, Kim J. *et al.* 1999, Kim *et al.* 2000). A localized point-like energy release, which is growing in time, should trigger the various phases of an unfolding dynamical instability on different timescales than a non-localized source of energy release. Therefore, the primary reason for our examination of isothermal models is to compare the dynamical features of the Parker instability driven by perturbing sources with a different character of the spatial and temporal distribution. Unlike the case of a non-localized linear perturbation, the SN explosion itself is a nonlinear dynamical process, and hence, under appropriate conditions, the two processes – the SN explosion and the Parker instability – can interact and amplify each other depending on the given time scales. Such an interaction can be better understood in simple isothermal models because the sound speed is spatially homogeneous and because the contaminating features which plague non-homogeneous (two temperature) media (see Section 4.2) do not appear.

The energy input which we apply in order to start the explosion and trigger the instability (see section 2) does not always correspond to a strongly nonlinear perturbation. Its relative magnitude can be estimated as the ratio $E/E_{\rm th}$, where $E_{\rm th} = (\gamma - 1)^{-1} k_B n_0 T V$, V being the volume of the perturbed region. For example, for $\gamma = 1.05$ and $V = 43^2 \times 1000$ pc^3, this is only $E/E_{th} \simeq 0.43$. Therefore, for $\gamma \sim 1$, the energy input $E = 2 \cdot 10^{51}$ erg does not correspond to a SN explosion but rather to a point-like nearly linear perturbation – most of the astrophysical details of a realistic energy input from a SN are left aside. It allows us, however, to understand how a Parker instability initiated by a weak localized perturbation develops under these basic assumptions.

We thus expect that when γ is small and the gravitational acceleration is less than $\approx 5 \cdot 10^{-9}$ cm s^{-2}), the growth rates for the Parker instability are much smaller than the existing growth rates for similar models, based on non-localized (sinusoidal) perturbations. The reason for this difference is that a point-like perturbation can initiate the instability only when it has propagated to overcritical spatial scales, and since for small γ the produced perturbation is weak and propagates with sound speed, it takes $t \sim \lambda_c/c_s$ Myr until the instability can start to grow. Moreover, the magnitude of the perturbation when it reaches overcritical scales is very small. On the other hand, a non-localized overcritical perturbation starts to grow directly at $t = 0$. When g becomes larger λ_c becomes smaller and the stratification becomes stronger. A localized perturbation can therefore propagate more rapidly up to the critical scale. Additionally, for larger γ, the perturbation increases and a shock wave can be produced. As a result, the instability is growing much faster, on scales comparable to those obtained for a non-localized perturbation.

4.1.1 Small γ, small g

The simulations performed in this category correspond to model 1Tg3 in table 1. The energy density contained in the perturbed region is $\delta\epsilon = 1.2 \times 10^{-11}$ erg cm^{-3}, while the background thermal energy density is $\epsilon = 2.76 \times 10^{-11}$ erg cm^{-3}. Therefore, the perturbation is only weakly nonlinear with a relative magnitude $\delta\epsilon/\epsilon \simeq 0.4$, by a factor of $\simeq 14$ less than for a monoatomic gas with $\gamma = 5/3$. In the initial stages, a sonic shock wave forms, which later becomes subsonic and propagates as a linear perturbation – a magnetosonic wave. The estimated time for the perturbation to reach a height equal to the critical wavelength in this case is about 126 Myr. In models with a sinusoidal perturbation, the Parker instability at this stage was already well into the nonlinear regime (see Mouschovias 1996, Matsumoto *et al.* 1988 for comparison). In our case, only after this time has passed, is the instability initiated. After 296 Myr, the Parker flow is well developed with maximum velocities at the footpoints of the loop of about $4c_s$ and an increase in thermal pressure at the foot points of the loop of up to one order of magnitude with respect to the initial values. The elevation of magnetic field lines, however, is not very prominent and a saturation is reached after 296 Myr.

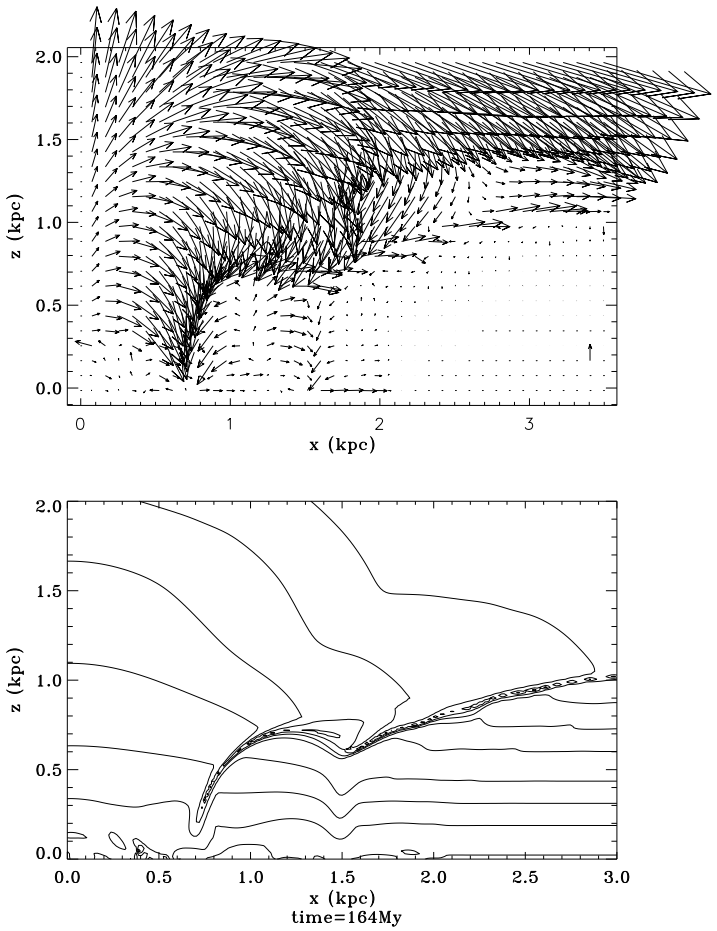

Figure 1. Velocity vectors in the $x-z$-plane (upper panel) and magnetic field lines (lower panel) for $t = 164$ Myr, $g = 6 \times 10^{-9}$ cm s^{-2} and $\gamma = 1.05$.

4.1.2 Small γ, large g

Model 1Tg4.5a. Here the gas scale height is smaller than in the previous case, and therefore the shock wave is stronger at given z. In addition, the critical wavelength is smaller in this case, so that the perturbation covers the scale of one critical wavelength after only 53 Myr. The supersonic flow sparks rapid growth of the Parker instability because the velocity and magnetic field perturbations are nonlinear: $v \gtrsim c_s$, $\delta B \gtrsim B_0$. At these stages, feedback features are observed in the dynamics of the outflow: due to the growing Parker instability, gas starts to slide downward along the field lines and the density in the upper parts of the expanding shell decreases. This allows for the hot bubble and the lightened shell to expand rapidly upward. However, due to this interaction between the two flows – the expanding gas and the Parker instability – the amount of mass ejected into the halo is smaller in comparison with the models where the instability cannot grow. The velocity of both the outflowing gas carried by the magnetic field loops, and the gas sliding downward along the loops, is strongly supersonic, reaching velocities of up to $5c_s$ (the plasma beta reaches 0.01 in the middle loop regions and 100 in the foot point regions, for all z.

Model 1Tg6. Due to the further decrease of the scale height, the amplitude of the magnetosonic wave is larger at a given z than in the previous cases, and when the wave reaches approximately $2H$ (at $t \sim 20$ Myr) it becomes supersonic. In $t \sim 43$ Myr the perturbation has propagated up to the actual λ_c and the Parker instability can grow. As seen in Fig. 1 at $t = 164$ Myr, the Parker flow is already well developed, so that the velocity profiles near the vertical symmetry plane show a self-similar behaviour, typical for the advanced stages of the Parker instability (Shibata *et al.* 1989), with the gas being accelerating upward. There is also evidence for a small secondary loop centered at $x = 1.2$ kpc with roughly the critical wavelength. In the next Section we will see that in the two temperature models, the effects of the self-propagating Parker instability (the formation of multiple loops) are more pronounced. The velocity vectors are normalised to the sound speed, which is represented in the lower right corner of the domain. After 164 Myr, the plasma beta has decreased by about two orders of magnitude with respect to the initial equipartition value. At the foot points of the loops, there is evidence for strong shock waves, built from gas sliding downward with supersonic velocities. These models tend to show that a larger gravitational acceleration, g, results in larger flow velocites for a given time and height and a stronger decrease of the plasma beta.

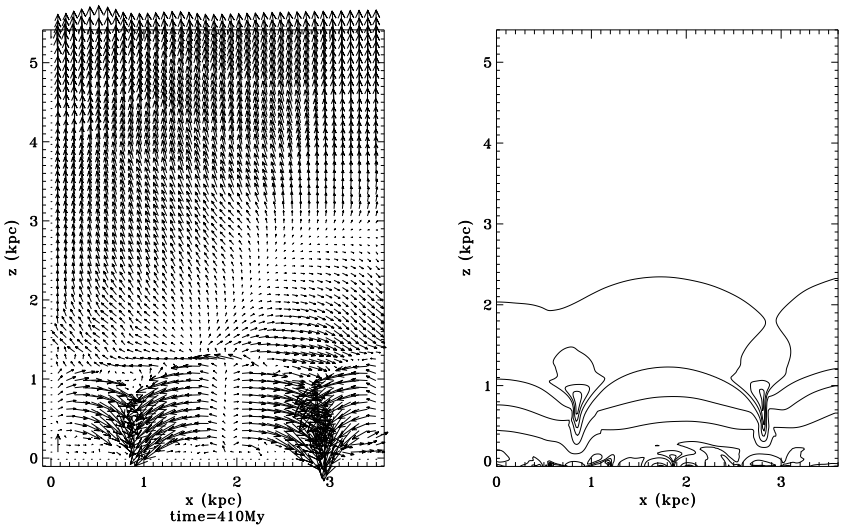

Figure 2. Velocity vectors in the $x-z$-plane (left panel) and magnetic field lines (right panel) for $t = 410$ Myr, $g = 3 \times 10^{-9}$ cm s^{-2} and $\gamma = 1.05$.

4.1.3 Large γ

Model 1Tg4.5b. When γ increases, the relative perturbation increases according to $\delta\epsilon/\epsilon \propto (\gamma - 1)$ (for $\gamma = 1.4$, $\delta\epsilon/\epsilon \simeq 3.6$). This means that the perturbation can drive a strong shock wave and forms a shell from the very beginning. Even though λ_c is very large in this case (about three times larger than for $g = 6 \times 10^{-9}$ cm s^{-2}), the perturbation propagates strongly supersonically and after $t = 40$ Myr, the scale of λ_c is reached and the instability can grow. Further expansion leads to acceleration of the shock and the postshock flow due to both exponential decrease of the density, and evacuation of gas from the upper regions of the shell. The associated Parker flow is already highly developed. Profiles of vertical velocity, in a narrow region close to the vertical symmetry plane, show signs of a self-similar behaviour which differs from the linear self-similar velocity profiles described by Shibata *et al.* (1989). We assign this difference to the interaction between the expanding shock and the Parker instability. By comparing models 1Tg4.5a and 1Tg4.5b, we can thus conclude that increasing γ while keeping the gravitational acceleration constant results in the flow displaying more vigorous dynamics. This is a direct consequence of the larger relative amplitude of the perturbation for larger γ.

4.2 Two temperature model

The observed HI density distribution (see Dickey & Lockman 1990), as well as the distribution of X-ray and radio-continuum emission (Kalberla & Kerp 1998) suggests that the ISM is intrinsically multi-component. For our purpose, the ISM can be reasonably described by a two temperature distribution with a warm disc and a hot overlying corona (see Shibata *et al.* 1989, Kamaya *et al.* 1996). In such models, new dynamical effects appear. On one hand, due to the large sound speed in the halo, the SN-triggered wave starts to propagate much faster when it reaches the interface. The parts of the wave front propagating along the interface therefore disturb the gas in the disc through associated perturbations of pressure, and thus, at a given time, the perturbation covers much larger distances in x than in the isothermal case. In general, the development of the Parker instability is favoured, and multiple loops are produced in the disc. On the other hand, due to the much larger scale height of the hot halo, the instability could saturate when the loops are entering this medium.

Kamaya *et al.* (1996) have obtained the strongest evolution of the SN driven Parker instability extending deep into the halo in their two temperature model. However, they adopted a specific heat ratio of $\gamma = 1.05$ for which, as we mentioned above, the relative perturbation is rather small and can be considered as weakly nonlinear point-like. In order to better understand how the system responds to nonlinear perturbations with larger relative magnitude, we have studied the effect of larger γ (including $\gamma > \gamma_c$). We have perfomed exploratory simulations for a wide range of parameter combinations, which are summarized in Table 2.

4.2.1 Low g

Model 2Tg3k1.05. In this case, the relative perturbation is weak, and thus the explosion front propagates with subsonic velocity up to 1-2 scale heights of the disc. Subsequent expansion in an exponential environment is accompanied by the amplification of the wave, which becomes supersonic when the front reaches a height of about 4H. In about 50 Myr, the perturbation has

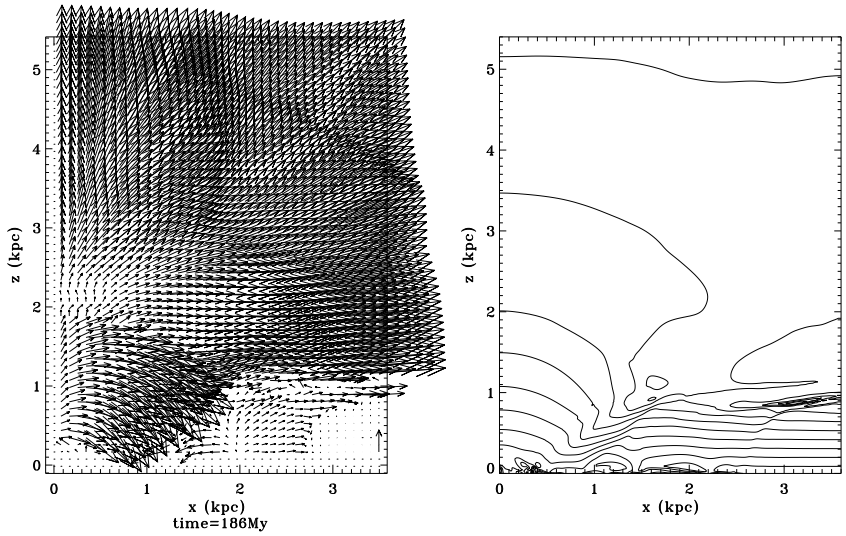

Figure 3. Velocity vectors in the $x-z$-plane and magnetic field lines at $t = 186$ Myr (lower panel) for $g = 4.5 \times 10^{-9}$ cm s^{-2} and $\gamma = 1.6$.

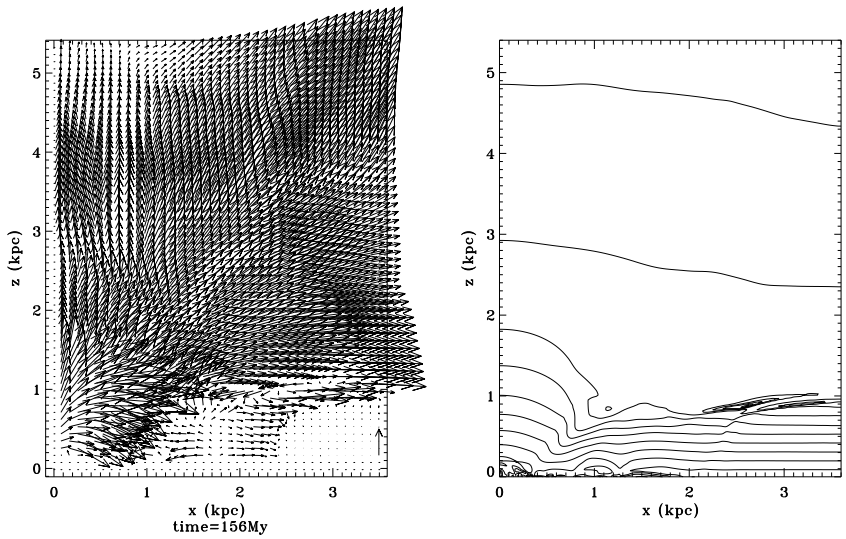

Figure 4. Velocity vectors (left panel) and magnetic field lines (right panel) at 156 Myr for $g = 4.5 \times 10^{-9}$ cm s^{-2} and $\gamma = 1.75$.

reached the interface between the disc and the halo, and in the following ~ 30 Myr, it covers a vertical range of ~ 3 kpc, while horizontally in the disc the critical wavelength is covered at this time. As a consequence, a weakly growing Parker instability is initiated with well defined loops building up in about 410 Myr, as seen in Fig. 2, which shows the velocity vectors and associated magnetic field lines. The vertical arrow in the left lower corner of the domain represents the sound speed, to which the velocity of the flow is related. While the wavelength of the main loop centered at about 2 kpc can be estimated to be about 2 kpc, which is close to the wavelength of maximum growth (see table 2), the two half-loops that are also seen in the picture have smaller wavelength. This difference is a consequence of the interplay between the applied nonlinear perturbation and the interface. The perturbation propagating faster in the halo than in the disc is disturbing the interface and is bei ng transmitted in this indirect way to the disc driving a propagating Parker instability: when it covers a horizontal distance comparable to the wavelength of maximum growth, the instability forms a loop in shortest time. To the contrary, the half-loop centered at the origin is initiated directly by the explosion, and is growing slower. This is a consequence of the implied nonlinear perturbation. The density increase in the valleys relative to the ambient medium for a given z reaches about a factor of 10. We want to emphasize, however, that this growth time is much larger than the typical growth times obtained as a result of sinusoidal perturbations (see Matsumoto *et al.* 1988, Mouschovias 1996, Kim *et al.* 2000), and depending on the rotation time of the galactic disc at the given distance from its centre, the instability might become irrelevant on interesting time scales. In addition, the elevation of magnetic field loops from the disc into the halo is not very significant, reaching out to at most 2 kpc.

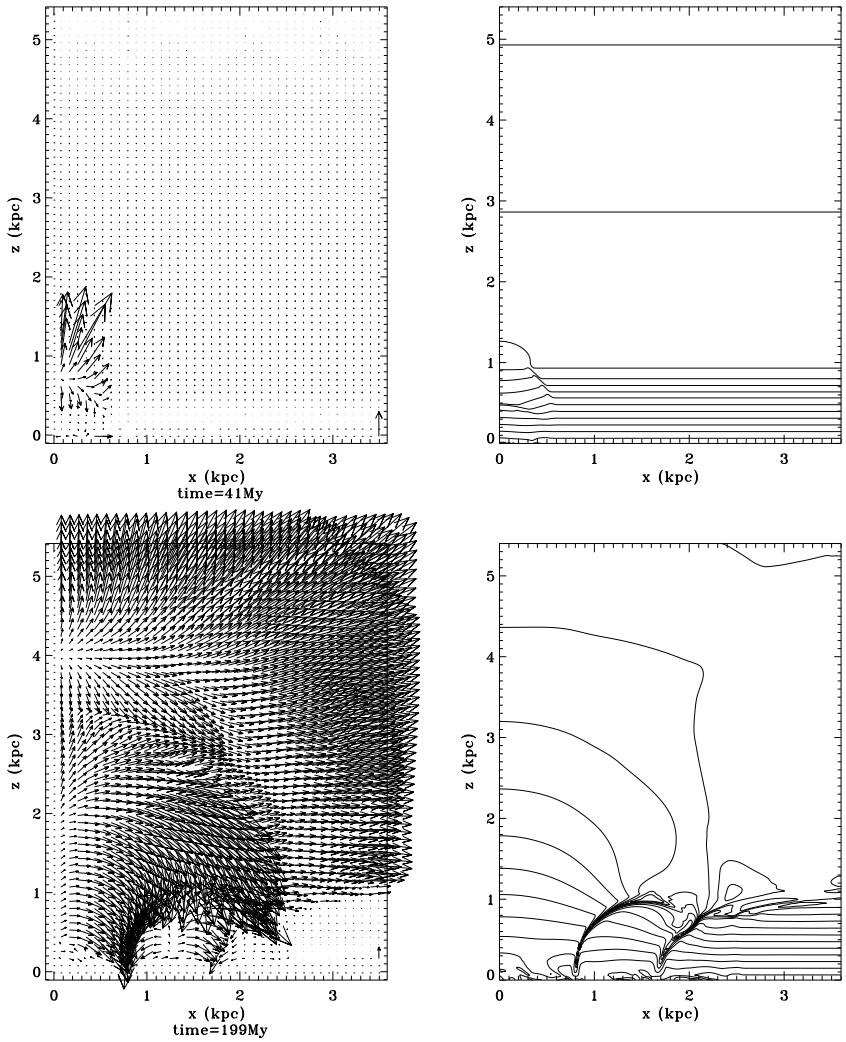

Figure 5. Velocity vectors and magnetic field lines at 41 Myr (bottom) and 199 Myr (top) for $g = 6 \times 10^{-9}$ cm s^{-2} and $\gamma = 1.05$.

Model 2Tg3k1.4. As γ increases, the perturbation also increases as described in the one-temperature models, and the flow is more strongly supersonic in both z and x. Even though the critical wavelength is larger in this case, it can be reached by the perturbation faster than in the case of lower γ. The simulations therefore reflect a smaller growth time than in the previous case, while the overall evolution of the system is very similar, including the formation of the secondary loops dicussed above.

For $\gamma = 1.75$, the Parker instability is not growing on relevant time scales, contrary to the case of larger gravitational acceleration, where, as discussed in the next section loops are still formed.

4.2.2 Medium g

The models with $g = 4.5 \times 10^{-9}$ cm s^{-2} are characterised by lower scale heights and critical wavelengths, and show faster evolution than for smaller gravitational acceleration as expected from linear analysis. In model 2Tg4.5k1.05, the initial relative perturbation is small, and the dynamics of the stimulated flow is similar to that in model 2Tg3k1.05, although more vigorous. The Parker instability therefore grows on shorter time scales. However, even for this stronger gravitational acceleration, significant loops with density enhancement in the pockets comparable to those obtained in the previous case are built only after 330 Myr. In the simulations with larger γ, models 2Tg4.5k1.4, 2Tg4.5k1.6 and 2Tg4.5k1.75, the initial relative amplitude of the perturbation becomes much larger so that shock waves form. Fig. 3, where we represent the velocity vectors and magnetic field lines at $t = 186$ Myr for $\gamma = 1.6$, shows the well developed Parker loops and associated gas flow. A second loop with a smaller wavelength is visible in this plot.

For $\gamma = 1.4$, the evolution is similar and the growth time is roughly the same. Subsequent time steps show the rising large-scale Parker loops reaching far out into the halo up to $z = 3$ kpc. In addition, the loops cause a radial outflow to be

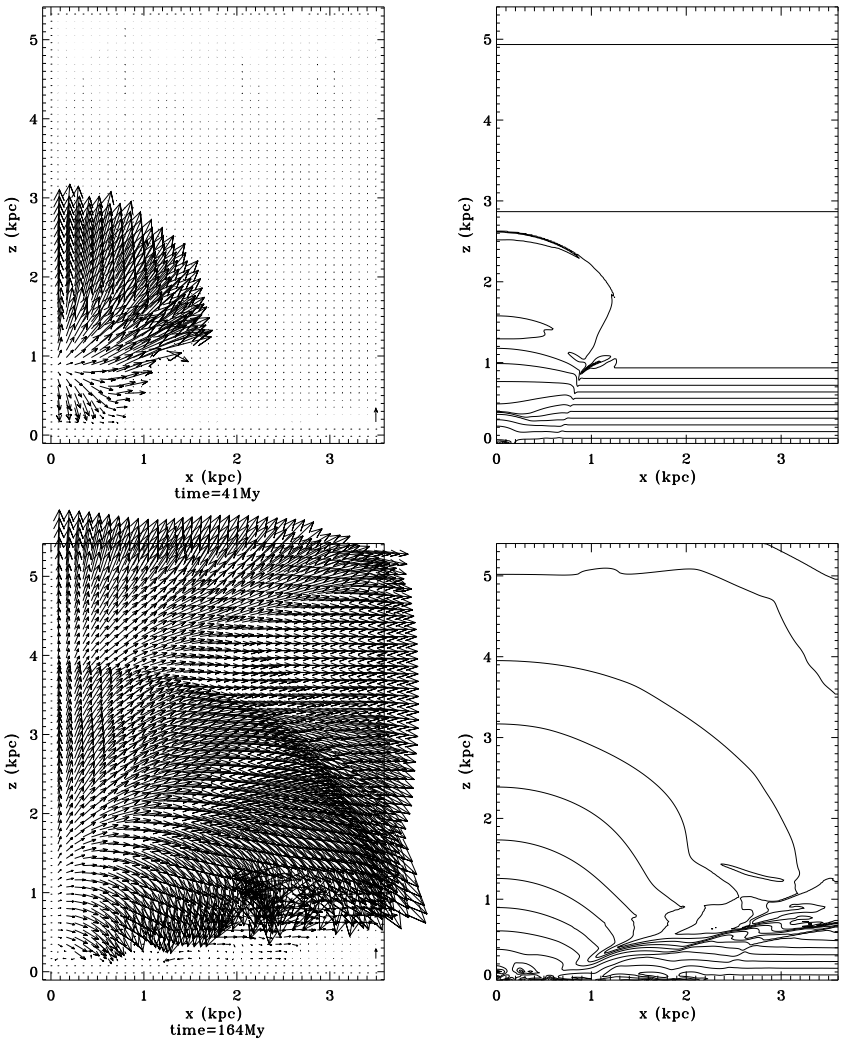

Figure 6. Velocity vectors and magnetic field lines at $t = 41$ Myr (top) and $t = 164$ Myr (bottom) for $g = 6 \times 10^{-9}$ cm s^{-2} and $\gamma = 1.6$.

driven ahead. For all γ, the largest vertical velocities are determined by the gas sliding down along the footpoints of the loops, and can reach $3c_s$ (where c_s is the sound speed in the disc, which we have represented in the lower right corner of the left panel).

In the linear theory, the Parker instability grows only when γ is less than the critical value $\gamma_c = (1+\beta^{-1})^2/(1+3\beta^{-1}/2)$, which for $\beta = 1$ is 1.6. For larger γ, MHD waves disperse the perturbation on time scales which are less than the free-fall time. When the disturbance is nonlinear, it can form and then maintain a localized structure which allows gas to slide down along the curved magnetic lines, and thus even for $\gamma \geq \gamma_c$, one can expect the Parker instability to grow. In the above-described model 2Tg4.5k1.6, both λ_c and λ_m are indefinite. At the same time, the critical value for γ has been derived in the theory of linear perturbations. However, for nonlinear perturbations the dispersion relation will change and γ_c is expected to change as well. Even in the model 2Tg4.5k1.75 we observe formation of loops, but on larger time scales compared to the previous two models. In Fig. 4, we show the velocity vectors and magnetic field lines for $t = 156$ Myr.

4.2.3 Large g

All three investigated models 2Tg6k1.05, 2Tg6k1.4 and 2Tg6k1.6 show vigourous growth of the Parker instability on scales less than or comparable with the rotation period of the galactic disc. In Fig. 5, we show the evolution of the instability for $\gamma = 1.05$. The upper panel shows the propagation of the perturbation at $t = 41$ Myr, while the middle panel is already representing the fully evolved instability after only 199 Myr. The main loop centred in the origin has roughly the size of the wavelength of maximum growth (see table 2) while the secondary loop already visible at this stage forms at about the critical wavelength.

For larger γ, the equivalent energy input is strong enough to lead to a supersonic shell when the front reaches the hot

halo. This can be seen in the lower panel of Fig. 6. The front is pushing a magnetosonic amplifying wave upwardly which soon becomes nonlinear and forms a secondary shell. Compared to $\gamma = 1.05$, the dynamics of the system is much more vigorous. The developed magnetic field structures are much more extended in x. We attribute this to the interaction between the Parker flow and the blow-out and to the larger critical wavelength. Secondly, the magnetic field lines show a more shell-like structure, indicating the presence of a strong radial outflow, which can be seen in the upper panel of Fig. 6 at $t = 164$ Myr. The maximum velocity of the flows reaches about $6c_s$.

5 DISCUSSION

In all cases we considered, the energy input E is always less than the minimal energy $E^B_{\rm min}$ required for a blow out by a factor 2–5 depending on g and γ, but larger than the minimal energy $E^P_{\rm min}$ needed for the Parker instability to grow on one rotational time t_R. We are thus in the range where the standard blow out does not operate, and the outflows produced by an explosion are connected with the growing Parker instability.

The explosions with $E \gtrsim E^P_{\rm min}$ initiate the nonlinear Parker instability during the later stages of their evolution. The growth time related to the rotation time of the galactic disc depends on the gravitational acceleration and the ratio of the specific heats. When the characteristic dynamical time for a weakened shock wave and the growth time for the Parker instability are comparable, the two processes interact. Even though the shock wave is transsonic (Mach number $M \sim 1$), it produces a nonlinear perturbation in the velocity and magnetic field, $v \sim c_s$ and $\delta B \sim B_0$, respectively. At these conditions the compression of gas and magnetic field and the Parker flow operate simultaneously. The Parker instability evacuates gas from upper parts of the magnetic loop, resulting in a faster expansion of the interior hot bubble, or the expanding bubble is carrying material away, allowing for the magnetic field to rise more easily and for the instability to grow faster. Due to this interaction, the shell looses mass. As a consequence, the total amount of gas which can be ejected into the halo is expected to be less than in cases when the Parker instability does not operate. At the same time, the magnetic loops formed by such flows must be more prominent and must extend further out into the halo. From this point of view, the structures built differ qualitatively from those which arise when the Parker instability is initited by a non-localized linear sinusoidal perturbation. In the latter case, a steady state appears to be reached and the loops extend up to ~ 1 kpc with respect to the plane (Kim *et al.* 2000). We can thus conclude that the origin of the large scale magnetic loops observed in haloes of edge-on galaxies might likely be connected with explosions in the underlying discs with the explosion energy lying in the range $E^P_{\rm min} < E < E^B_{\rm min}$. Assuming the luminosity function of OB associations to be universal (a power-law, Williams & McKee, 1997) one can expect that large scale magnetic arches must be more numerous in galaxies with larger gravitational acceleration g, as both $E^P_{\rm min}$ and $E{\rm min}^B$ decrease with g.

Although we have not considered the limit $E > E^B_{\rm min}$, we expect the hot bubble and the shell to expand much faster than the Parker instability evolves, so that the effects of removal of gas from the shell can be neglected, and the total amount of mass ejected into the halo is comparable to that expected for explosions in a non-magnetic ISM. Such explosions also produce large scale magnetic arches in galactic halos. However, in this case, a much larger amount of gas must be associated with the loops in comparison with explosions having smaller energies. It is evident that magnetic structures of this kind must be less numerous in galactic halos since $E^P_{\rm min} < E^B_{\rm min}$.

We conclude that the ejection of mass and magnetic fields into the galactic haloes due to blowing out SNe explosions is most efficient in galaxies with large gravitational acceleration g. Consequently, galaxies with large g must have more massive halos (relative to the mass of their gaseous discs), smaller scale heights, and more prominent large scale magnetic arches. Assuming that the gas mass in galactic halos is proportional to the number of OB associations with the SNe energy larger than $E^B_{\rm min}$, and that the luminosity function of associations is universal, one can expect the mass of the halo gas to vary as proportional to g^3. By comparing the energy limits $E^P_{\rm min}$ and $E^B_{\rm min}$, one can conclude that the large scale magnetic Parker loops in the halo of a given galaxy must be more numerous than the blow-out events. From the observational point of view, these structures differ from each other mainly by their plasma β parameter: in blow-out flows $\beta \sim 1$ since the frozen-in magnetic field is compressed by a gas flow that is predominantly transverse, while in magnetic loops formed due to the Parker instability, $\beta \ll 1$, since the gas flow here is predominantly longitudinal (Mouschovias 1974). However, in order to distinguish these structures, one needs to measure both the strength of the magnetic field and the gas pressure in galactic halos, which is beyond the present observational possibilities.

In all cases, we assumed equipartition between thermal and magnetic pressure for the unperturbed background state. However, both the critical wavelength and the characteristic growth rate for the Parker instability depend on β: for a fixed γ the critical wavelength becomes infinite and the instability does not develop when β is larger than a critical value $\beta_c(\gamma)$. The growth rate decreases in the limits $\beta < 1$ and $\beta > 1$ and reaches a maximum around $\beta \sim 1$. One can therefore expect that in galaxies where the equipartition between thermal and magnetic pressures is not given, the Parker instability is supressed, and only blow-out flows can occur, provided the energy input from SNe explosions is large enough $E > E^B_{\rm min}$.

All the above conclusions have been drawn from 2D studies of the Parker instability. In a 3D treatment, the growth of

small wavelength perturbations due to the manifestation of the interchange mode may change the dynamics of the system. Kim et al. (1998) have shown that the nonlinear phase and the final structures of the Parker instability in 3D can be different from those in 2D simulations. However, one has to bear in mind that they have assumed equipartition between thermal and magnetic pressure in the initial state and the linear growth of the Parker instability in 3-D, when the magnetic pressure is large compared to the thermal pressure is very different from the situation when beta is uniy. Based on this later assumption, they have demonstrated that in the planes perpendicular to the direction of the magnetic and gravitational field, the flow can be characterized as chaotic, while in the plane that contains the magnetic and gravitational field, the structures produced by the undular mode are still present and persist over a period of about 40 H/c. This time translates into about 400 Myr in our model for $g = 6 \times 10^{-9} cm/s^2$ an would leave enough time for the interaction we are concerned with to operate in 3D as well. Apart from this aspect, we study the evolution of the instability under a strongly nonlinear perturbation, the SN explosion. Compared to randomly applied perturbations, which are associated with equally distributed power in all possible wavenumbers, this perturbation has most of its power in the low wavenumber modes. The large wavenumbers favoured by the interchange mode will grow as well, but it will take longer for them to reach dynamically significant amplitudes. In addition they will be masked by the supersonic motions associated with the SN explosion and later the supersonic motions of the undular mode. Since our system is more complicated than the usual picture in which linear perturbations are used, it is not possible to completely infer the evolution of such a system from purely intuitive arguments. 3D simulations of the SN explosion induced Parker instability will provide us with the final answer and we will address this issue in a forthcoming work.

6 SUMMARY

In this paper our primary interest has focused on the evolution of the Parker instability induced by a single SN explosion. We have explored the dependence of the instability on the gravitational acceleration in the host galaxy and the ratio of specific heats, while we kept the energy input of the explosions as well as the volume in which this energy was distributed constant. It was our aim to address the question of how the energy input from an explosion converts into large scale motions corresponding to the Parker flow, depending on the gravitational acceleration in a host galaxy. Our results can be summarised as follows:

1. The question of whether the Parker instability triggered by a single SN explosion can lead to the observed large scale magnetic field loops in the halos of galaxies is strongly connected to the strength of the gravitational acceleration in the host galaxy, the energy of the explosion and the ratio of specific heats. We found that for values of the gravitational acceleration less than 4.5×10^{-9} cm s^{-2}, the instability is growing on much larger time scales in comparison to the models where a sinusoidal perturbation was applied in order to trigger the instability. The relevance of the instability in this case must be judged by relating its growth time to other dynamically important time scales (e.g. the rotation time of the galactic disc at the given distance from its centre). For larger g (around 6×10^{-9} cm s^{-2}) the growth rates for the instability are comparable to the models with nonlocalised perturbations. In this case, we obtained large growth rates for the instability. We conclude that in galaxies with large g in the disc, the Parker instability is relevant on dynamical time scales.

2. The choice of $\gamma > 1$ is equivalent to a larger amplitude of the localised perturbation and leads to larger growth rates of the instability. We obtained significant growth even for γ larger than the critical value $\gamma_c = 1.6$ known from the linear theory. This result is in agreement with the results obtained by Kamaya et al. (1996). One reason for this apparently contradictory behaviour is the applied nonlinear perturbation which changes the dispersion relation, and therefore the growth rate of the instability. The linear critical γ therefore should no longer be valid in this case. On the other hand, strong nonlinear perturbations are unaffected by the dispersive properties of the background medium.

3. Even one SN explosion can lead to the formation of multiple loops due to the fact that the perturbation propagates in the disc. The secondary loops in general are associated with smaller growth rates.

4. The SN explosion and the Parker instability are two dynamical processes that can interact and can influence each other depending on the given energetics, *i.e.* the minimal energy E^P required for the Parker instability to be initiated and the minimal energy E^B for the blow-out. In general, we distinguish three cases: a) If $E^P < E << E^B$ the observed magnetic structures are a consequence of the Parker instability; b) For $E^P < E \lesssim E^B$ the two processes interact and the resulting structures are a consequence of this interaction; c) For $E > E^B$ the ejection of mass and magnetic field into the halo is mainly due to the blow-out flow. Our simulations are only adressing case b). Observed outflow rates should reflect these three regimes. The dependence of the dynamics of the system on g can be converted into the dependence on the input energy via the scaling laws Eg^2 =const in the 2D case and Eg^3=const in 3D.

We thank D. Bomans, R.-J. Dettmar, V. Korchagin and A. Schröer for valuable discussions and the referee, Tom Hardquist, for his careful reading of the manuscript and critical comments. The authors acknowledge financial support from the German Science Foundation (DFG) within Sonderforschungsbereich 191.

REFERENCES

Appenzeller, I. 1974, A & A, 36, 99
Bahcall, J. N. 1984, ApJ, 276, 169
Basu, S., Mouschovias, T. Ch., Paleologou, E. V. 1997, ApJ, 480, L55
Bernstein, I. B., Kulsrud, R. M. 1965, ApJ, 142, 479
Bottema, R. 1995, The stellar kinematics of galactic disks, PhD thesis, Rijksuniversiteit Groningen
Brinks, E., Bajaja, E. 1986, A & A, 169, 14
Dettmar, R.-J. 1992, Fund. Cosmic Phys., 15, 143
Dickey J. M., Lockman F. J., 1990, ARA& A, 28, 215
Duric, N., Seaquist, E. R., Crane, P. C., Bignell, R. C., Davis, L. E. 1983, ApJ, 273, L11
Ferrara, A., Tolstoy, E. 2000, MNRAS, 313, 291
Ferriére, K. M., Mac Low, M.-M., Zweibel, E. 1991, ApJ, 375, 239
Giuliani, J. N. 1982, ApJ, 256, 624
Giz, A. T., Shu, F. H. 1993, ApJ, 404, 185
Heiles, C. 1984, ApJS, 55, 585
Horiuchi, T., Matsumoto, R., Hanawa, T., Shibata, K. 1988, PASJ, 40, 147
Howk, J. C., Savage, B. D. 1997, AJ, 114, 2463
Howk, J.C., Savage, B.D. 1999, AJ 117, 2077
Hummel, E., van Gorkom, J. H., Kotanyi, G. G. 1983, ApJ, 267, L5
Kalberla P. M. W., Kerp J., 1998, A&A, 339, 745
Kamaya, H., Horiuchi, T., Matsumoto, R., Hanawa, T., Shibata, K., Mineshige, S. 1997, ApJ, 486, 307
Kamaya, H., Mineshige, S., Shibata, K., Matsumoto, R. 1996, ApJ, 458, L25
Kim, J., Franco, J., Hong, S. S., Santillan, A., Martos, M. A. 2000, ApJ, 531, 873
Kim, J., Hong, S. S. 1998, ApJ, 507, 254
Kim, J., Hong, S. S., Ryu, D. 1997, ApJ, 485, 228
Kim, J., Hong, S. S., Ryu, D., Jones, T. W. 1998, ApJ, 506, L139
Kim, J., Ryu, D., Jones, T. W., Hong, S. S. 1999, ApJ, 514, 506
Kim, S., Dopita, M. A., Staveley-Smith, L., Bessel, M. S. 1999, AJ, 118, 2797
Kovalenko, I. G., Shchekinov, Yu. A. 1985, SovA, Astrophysics, 1985, 23, 578
Kuijken, K., Gilmore, G. 1989, MNRAS, 239, 605
Kulsrud, R. M., Bernstein, I. B., Kruskal, M., Fanucci, J., Ness, N. 1965, ApJ, 142, 491
Lamb, H. 1932, Hydrodynamics, CUP, Cambridge
Mac Low, M.-M., Ferrara, A. 1999, ApJ, 513, 142
Mac Low, M.-M., McCray, R. 1988, ApJ, 324, 776
Mac Low, M.-M., McCray, R., Norman, M. 1989, ApJ, 337, 776
Martin, C. L. 1996, ApJ, 465, 680
Matsumoto, R., Horiuchi, T., Shibata, K, Hanawa, T. 1988, PASJ, 40, 171
Matsumoto, R., Tajima, T., Shibata, K., Kaising, M. 1993, ApJ, 414, 357
Meurer, G. R., Freeman, K. C., Dopita, M. A., Cacciari, C. 1992, A J, 103, 60
Mineshige, S., Shibata, K., Shapiro, P. R. 1993, ApJ, 409, 663
Mouschovias, T. 1974, ApJ, 192, 37
Mouschovias, T. 1996, in Solar and Astrophysical Magnetohydrodynamic Flows, Kluwer Academic Publishers, Dordrecht, p. 475
Newcomb, W. A. 1961, Phys. Fluids, 4, 391
Oort, J. H. 1960, Bull. Astr. Inst. Netherlands, 15, 45 B
Palouš, J., Franco, J., Tenorio-Tagle, G. 1990, A & A, 227, 175
Parker, E. N. 1966, ApJ, 145, 811
Parker, E. N. 1967, ApJ, 149, 535
Parker, E. N. 1979, Cosmic Magnetic Fields, Oxford University Press, Oxford
Puche, D., Westpfahl, D., Brinks, E., Roy, J.-R. 1992, AJ, 103, 1841
Scalo, J. M. 1985, in: Protostars and Planets II, Tucson, AZ, University of Arizona Press, p. 201
Shibata, K., 1996, in Solar and Astrophysical Magnetohydrodynamic Flows, Kluwer Academic Publishers, Dordrecht, p. 232
Shibata, K., Tajima, T., Matsumoto, R., Horiuchi, T., Hanawa, T., Rosner, R., Uchida, Y. 1989, ApJ, 338, 471
Sofue, Y., 1976, A& A, 48, 1
Sofue, Y., Handa, T. 1984, Nature, 310, 568
Sofue, Y., Tosa, M. 1974, A & A, 36, 237
Sofue, Y., Wakamatsu, K.-I., Malin, D. F. 1994, AJ 108, 2102
Stone, J.M., Norman, M. L. 1992a, ApJS, 80, 791
Stone, J.M., Norman, M. L. 1992b, ApJS, 80, 819
Tenorio-Tagle, G., Bodenheimer, P., Rozyczka, M. 1987, A & A, 182, 120
Tomisaka, K. 1990, ApJ, 361, L5
Tomisaka, K. 1998, MNRAS, 298, 797
Tomosaka, K., Ikeuchi, S. 1986, PASJ, 38, 697
Tüllmann, R., Dettmar, R.-J. 2000, A& A, 362, 119
van der Kruit, P. C., Searl, L. 1981, A& A, 95, 105
Walter, F., Brinks, E. 1999, AJ, 118, 273
Williams J. P., McKee, C. F. 1997, ApJ, 476, 144
Ziegler, U., 1995, PhD, University of Wuerzburg

Ziegler, U., Rüdiger, G. 2000, A & A, 356, 1141